Next Materials 5 (2024) 100224

Contents lists available at ScienceDirect

Next Materials

journal homepage: www.sciencedirect.com/journal/next-materials

Research article

Hafnium dinitride/poly(9-vinylcarbazole) heterojunction: Structural, electronic, optical and vibrational properties. A DFT and DFPT study

V.W. Elloh [a,b,*], A. Yaya [c], Eric K.K. Abavare [d,**]

[a] Department of Biomedical Engineering, Koforidua Technical University, Koforidua, Ghana
[b] Department of Physics, University of Petroleum and Energy Studies (UPES), Dehradun, India
[c] Department of Materials Science and Engineering, University of Ghana, Legon, Ghana
[d] Department of Physics, KNUST, Kumasi, Ghana

ARTICLE INFO

Keywords:
Hafnium dinitride
Optical
Poly(9-vinylcarbazole)
Nanoheterostructure
Photocatalysis

ABSTRACT

Photosensitivity of semiconducting polymers can be enhanced by blending donor and acceptor polymers to optimize photoinduced charge separation. With a motivation to understand microscopic aspects of HfN_2 and PVK relevant to optoelectronic properties of transition metal-dinitride/semiconductor interfaces, we examined their structural, electronic, optical and vibrational properties using first-principles calculations based on density functional theory (DFT) and density functional perturbation theory (DFPT) levels of theory. We computed a large direct energy gap of 3.751 eV for PVK and an indirect narrow band gap of 1.396 eV in HfN2. The gap value computed for the composite structure, HfN_2/PVK, was 0.958 eV. The heterojunction displayed an indirect energy gap. The charge transfer between HfN_2 and PVK results in a polarized field within the interface region, which will benefit the separation of photogenerated carriers. The calculated density of electronic states, Lowdin charge transfer and charge density difference certify that this proposed layered nanoheterojunction is an excellent light-harvesting semiconductor. These findings indicate that the conjugated polymer PVK is a promising candidate as a non-noble metal co-catalyst for HfN_2 photocatalysis. It also provides useful information for understanding the observed enhanced photocatalytic mechanisms in experiments.

1. Introduction

It is well known through scientific researches and daily observations that CO_2 concentration has increased in our environment. There is depletion of fossil fuel, there is global warming, etc. All the above are as a result of over exploitation of the natural environmental resources to meet energy demands. This calls for seeking new green alternatives urgently to meet man's energy demands. As a means to curbing the energy menace, devices for harnessing solar energy into electric power has become even critical and seen as a necessary step in the right direction to combat global energy demands. Organic solid-state devices based on silicon as the sole source of power for a single junction device has been overrun by solar cell industries in the last few decades and it is still growing.

It is known that Si-based devices are very expensive to manufacture because of high purity demand of crystalline semiconductors. Alternatively, efforts have been shifted towards low-cost solar cells development. Photovoltaic cells based on nanoparticle materials and conducting polymers are new generations of such devices. Optical band gap tunability, processability, flexibility and cheap fabrication features characterize these devices. Conducting polymers have very high optical absorption coefficients compared to silicon and are suitable for manufacturing very thin solar cells.

Optoelectronic devices including organic photovoltaics, photodetectors and light-emitting diodes [1,2] have their operational efficiencies heavily relying on charge transfer processes at organic interfaces. The suitability of donor–acceptor interface is a quantum boost for efficiency in organic solar cells. This is a driving force or benchmark for organic solar cell industries [3,4]. Organic solar cell power conversion efficiencies in the 19–23 % range are due to efficient separation of excitons formed in the semiconductor at the donor–acceptor junctions [5–22]. There still remains limiting factors such as optical absorption, exciton dynamics, charge carrier mobility and its collection at the electrodes which impedes efforts to maximize

* Corresponding author at: Department of Biomedical Engineering, Koforidua Technical University, Koforidua, Ghana.
** Corresponding author.
E-mail addresses: vanw.elloh@ktu.edu.gh (V.W. Elloh), eabavare@yahoo.com (E.K.K. Abavare).

https://doi.org/10.1016/j.nxmate.2024.100224
Received 15 December 2023; Received in revised form 24 April 2024; Accepted 1 May 2024
Available online 21 May 2024

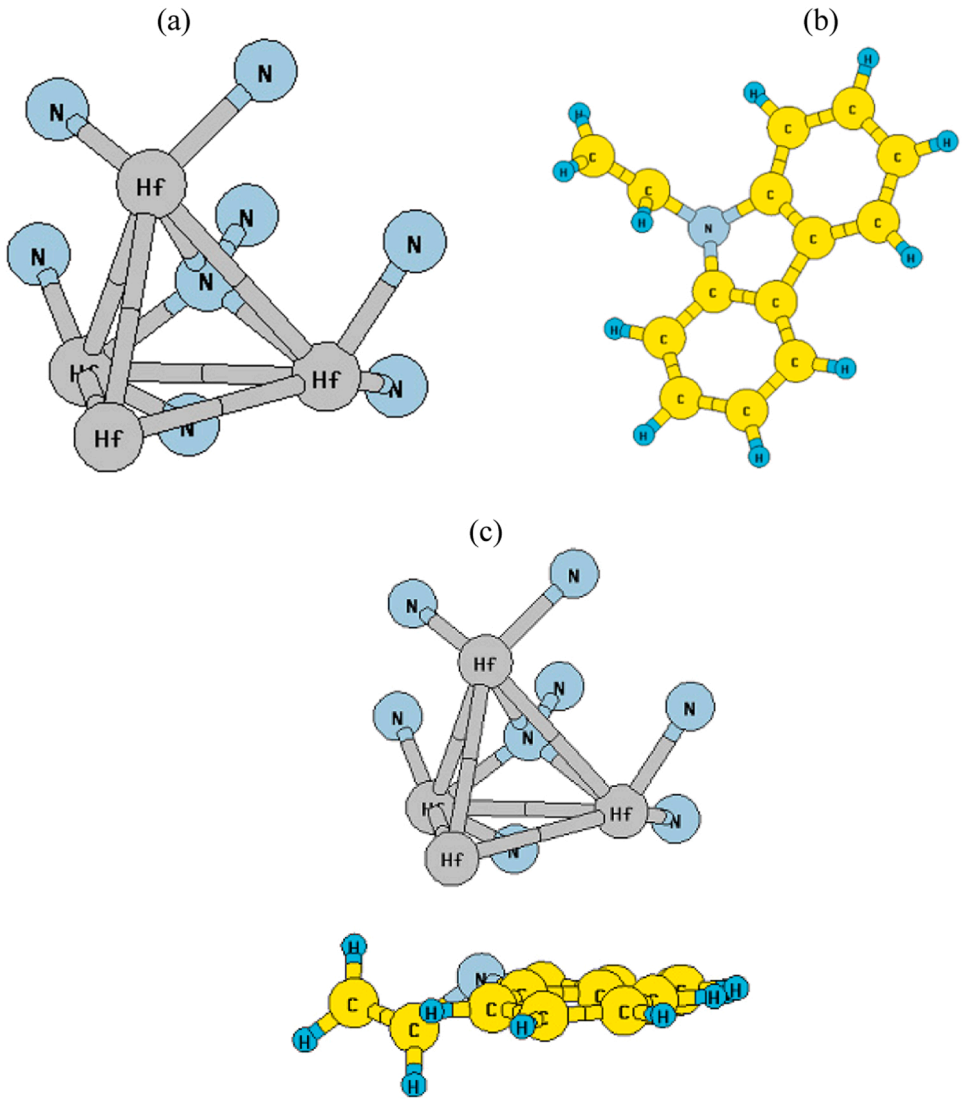

Fig. 1. (a) HfN_2, (b) PVK monomer, (c) HfN_2/PVK heterostructure.

performance. The various steps that have been taken to maximize efficiency includes thin planar multilayers or blends of polycrystalline or amorphous films to enlarge donor–acceptor contact area and to reduce the exciton path [23,24].

Heterojunction thin films derived from polymers including inorganic nanoparticles have become added advantages to organic materials for elevated mechanical pliancy, versatile functionality, modest and facile coating techniques. Unadulterated polymers having well defined HOMO and LUMO are engineered by prepending inorganic nanoparticles to realize novel-hybrid spectrum of absorption compatible with optoelectronic usages. The broad area of interface allying polymer-matrix/donor versus nanoparticle/acceptor energizes transfer of energy between carriers of charges, excitons at interface of inorganic–organic nanoarchitectures [25,26]. Controlling morphology of active layer improves photovoltaic cell performance.

Organic-inorganic interactions in hybrid structures of this type result in novel nanoarchitectures having prospective implementations in mechano-devices, optoelectronics, biosensors, CO_2 conversion and utilizations in magnetic-fields. Examples of hybrid materials of these kinds are nanowire manufactured from polymers of carbon including graphene which is derived from polymer heterojunctions. Preparation technique selection is paramount to realizing appropriate properties of nanomaterials. To maximize photosensitivity of semiconducting polymers we need to blend donor and acceptor polymers in such a way as to optimize photoinduced charge separation.

In the past few years, a great deal of research work has been done on poly N-vinyl carbazole (PVK). This is due to its chemical structure noted to be simple. PVK is known to be characterized with stable resistance nature, hole-transporting, large emission spectrum and long π-conjugation. Potential areas in optoelectronics where PVK utilization is in high demand includes light emitting diodes, FETs, biosensors and optical-detectors. Both theoretical and experimental works revealed PVK as a potential candidate to be employed in photovoltaic industries [27–32].

Transition metal mononitrides have some kind of superior physical properties. Their hardness, mechanical strength, high melting points and electrical conductivity properties transform from that of a metallic conductor to a semiconductor. By virtue of the above properties, they have found use in technological applications for hardware-resistant coatings, diffusion barriers and optical coatings. They are also under scrutiny to understand their potentials for use in areas like thermoelectricity. In search for alternative clean energy employing thermoelectricity, researchers believe that nitrides can play some important role in thermoelectric devices at high operating temperatures where the refractory properties of the nitrides will be advantageous. In this paper, we adopt DFT and DFPT levels of theory to study the optical absorption spectrum, exciton diffusion and charge carrier dynamics of a novel

hybrid material HfN_2/PVK nanoheterojunction.

2. Computational details

Calculations were performed using plane wave self-consistent field (PWSCF) implementation within the framework of density functional theory (DFT) employing the simple local density approximation (LDA), parameterized by Perdew and Zunger [33], and the generalized gradient approximation (GGA) of Perdew, Burke and Ernzerhof (PBE) [34]. The Vanderbilt Ultrasoft Pseudopotentials scheme [35] was employed. The Kohn-Sham orbitals were expanded in a plane-wave basis set. Ultrasoft pseudopotentials represent the interaction between ionic cores and valance electrons. We adopted the supercell model for HfN2/PVK nanoarchitecture. The supercell was oriented along the z-axis and unit cell geometry with a vacuum space of 15 Å thick in both x- and y-directions were allowed to ensure negligible interactions between the supercell and its periodic images. Plane wave cut-off energy of 30 Ry was used to represent the electronic wave functions. Plane wave energy of 180 Ry was included for the description of charge density. Integration over the Brillouin zone is carried out using the Monkhorst–Pack scheme [36] with a $10 \times 10 \times 10$ mesh of k-points. Occupation numbers were treated according to the Methfessel–Paxton [37] scheme with a broadening of 0.003 Ry. Quantum Espresso, an electronic structure calculation code [38] was utilized in the determination of the electronic structure of HfN_2/PVK interface. A minimum interlayer interaction distance, d_{min} $\sim$ 3.323 Å was kept between the HfN_2 and PVK molecules throughout the computations. The calculated interlayer distance is comparable to graphite interlayer separations (ca. 3.35 Å).

Time-dependent density functional perturbation theory (TDDFPT) was employed in the computations of optical absorption spectra of the modeled heterointerface. We performed a self-consistent-field ground-state calculation for the molecule at the equilibrium structure using the standard plane-wave program. In this case, the k-point sampling is restricted to Γ-point only. For the purposes of comparison, Turbo-Davidson and Liouville-Lanczos programs were utilized to compute optical absorption spectra of the modeled molecule.

Lattice-dynamical calculations for phonon spectrum and density of states were performed within the framework of the self-consistent density functional perturbation theory (DFPT) [39]. Plane wave cut-off energies of 30 and 650 Ry were used to describe wave functions and charge density, respectively. Such a high charge density cut-off is necessary to keep the errors in vibrational frequencies minimal. In order to understand the detailed features of the phonon spectra, force constants were obtained on a $4\times4\times4$ q-point mesh. The dynamical matrices at arbitrary wave vectors were obtained using Fourier transform based interpolations.

3. Discussions of results

3.1. Unit cell of HfN_2 and PVK structures

HfN_2 is a hexagonal structure with *P-m*2 symmetry and space group number 187 and forms six (6) trigonal prismatic structural geometry. The central Hf atoms are surrounded by six nearest N atoms and this extends to occupy all space.

Transition metal dinitrides (TMDNs) have extensively been studied due to their excellent physical and mechanical properties. First principles-based calculations have also predicted the structural existence and stability of TiN_2 of these refractory compounds at high pressures when TiN and dense N_2 gas was used as percussor and has since been confirmed by experimental studies. This breakthrough has attracted a lot of researchers to TMDNs compounds research [40,41].

Thin film HfNx has been successfully synthesized through silicon technology (TSV) method with the bulk showing superior ductility [42]. Sun et al. have theoretically predicted the stability of HfN_2 [43], the mechanical and electronic properties of the compound have similarly been carried out for device application using DFT [44–46]. The HfN_2 compounds have excellent valley polarization properties and good candidates for device applications especially in valleytronics and spintronics devices [47,48]. In the ultraviolet energy region of the electromagnetic spectrum, HfN_2 has high absorption coefficient and there exists the possibility that the material could be used in UV-photodetectors in this region. The measure of harvesting thermoelectric energy is determined by the thermoelectric figure of merit value. 2D HfN_2 having such a high value makes it a potential candidate for harnessing thermoelectric energy. Poly(9-vinylcarbazole) is usually characterized as conjugated polymer, temperature-resistant, photoconductive and hole transporting [49–54] (Fig. 1).

Table 1
Computed results for bandgap E_g(eV), difference in energy E_0(eV) for PVK, HfN_2 and HfN_2/PVK (ca. [60]).

	a/Å	b/Å	c/Å	E_g/eV	E_0/eV
PVK	4.451	4.451	2.423	3.751	4.083
HfN_2	5.128	5.128	5.128	1.396	3.047
HfN_2/PVK	7.402	6.218	7.551	0.958	0.00
HfN_2/CrI_3	6.930	6.930	–	0.810	

Carbazole polymers consist of carbazole and pendant groups with the carbazole group as its backbone. A key member of the carbazole polymer is those with the conjugated group and the N-vinylcarbazole is the most important class of them [55–57]. The poly(N-vinylcarbazole) (PVK) polymer is of interest because of their excellent photoconductive properties making them potentially suitable for applications in electrophotography, organic photorefractive, polymeric light-emitting diodes and photovoltaic devices.

The relatively high dielectric properties associated with this PVK found its earlier electronic uses in capacitors and other applications and as a consequence, its associated complex in transferring charge within trinitrofluorenone (TNF) was introduced commercially as electrophotography [58].

One of the most widely known photoconductor is polymeric PVK material and is used in combination with TNF photocopiers. Nevertheless, the use of PVK/TNF system has been found to have low photosensitivity. Again, it is also known that TNF films are highly toxic with poor mechanical strength indicating that, a much more superior materials are required.

There is inductive effective emanating from the nitrogen atom attached to the vinyl group which tend to lower the electron density distribution on the vinyl group. Consequently, electron lone-pair on nitrogen mesomeric effect tends to overcome vinyl-group inductive effect leading to the formation of the conjugated π-electron system.

3.2. Property structure

We studied the geometry and structural stability of PVK interacting with HfN_2 using nanoheterojunction supercell model for the calculations. Series of geometrical orientations and stability of PVK polymer chain interacting with HfN_2 monomer have been considered. The PVK polymer chain was oriented apace with the HfN_2 monomer, the functional species either pointing to or inversely from the HfN_2 monomer. The PVK chain was curved around the HfN_2 monomer and flipped 180° about its center. The preferrable alignment of the PVK polymer chain was when its side groups pointed towards the HfN_2 monomer. This pattern resulted in the lowest enthalpy of formation. This is energetically stable and favorable so it was utilized in the study. A vacuum space of $\sim$ 3.383 Å was maintained between HfN_2 and PVK monomer throughout the study. Table 1 shows energy difference values, E_0(eV), for PVK, HfN_2 and HfN_2/PVK. HfN_2/PVK displays structural stability over PVK and HfN_2. Computed bandgap energy values, optimized lattice parameters and structural values are depicted in Table 1. Eqs. (1) and (2) were adopted for the structural stability computations for the

Table 2
Optimized **N-C**— & **N-Hf**— bond-length (Å) of the Novel Nanoheterostructure.

	Bond-length (Å)	
	N — N	N — Hf
Before	1.5145	2.2149
After	1.3951	2.1021

Table 3
Adsorption energy, E_{ad}, formation energy per atom, E_{pa}, computed from relations 1 & 2.

Structure	$\mathbf{E_{ad}}/eV$	$\mathbf{E_{pa}}/eV$
PVK		− 5.263
HfN_2		− 1.055
HfN_2/PVK	2.236	− 7.933

heterojunction. We computed the adsorption energy, E_{ad}, and recorded the outcome in Table 2. The relation (1) below, [59] was used in the calculations.

$$E_{ad} = \left(E_{PVK/HfN_2} - E_{PVK} - E_{HfN_2}\right) \quad (1)$$

Where E_{PVK/HfN_2}, E_{PVK}, E_{HfN_2} are the HfN_2/PVK composite's total energy in its ground-state; the PVK total energy in the ground-state and HfN_2 total ground-state energy respectively. In the process of geometry optimization, the value of dispersion contribution to total energy at various stages is reported by the Quantum Espresso code. To obtain adsorption energy dispersion contributions, Eq. (1) was employed. We replaced the right-hand side terms with appropriate dispersion quantities for the converged geometry for each structure. For the surface adsorption to be thermodynamically feasible, the adsorption energy must be positive. This means that the greater the E_{ad} value, the stronger the binding of the HfN_2/PVK interface. Careful observation of Table 2 depicts how favorably it is for the HfN_2 molecule to adsorb onto the PVK monomer surface. Our calculated adsorption energy value was found to be 2.236 eV. There is chemisorption between the carbazole unit and the HfN_2 at the surface of the HfN_2/PVK composite. The contributing factors are the presence the of nitride functional groups in the conjugated polymer-chain, the interactions between the π-electrons of the polymeric chain and the strong π-π interactions between the carbazole unit and the HfN_2. The relation (2) below was used for formation energy computations. The calculated energy of formation, E_{pa}, in HfN_2 was found to be − 1.055 eV. The energy of formation in PVK was also computed, the value turned out to be −5.263 eV.

$$\Delta E = E_{CHfN} - N_C E_C - N_{Hf} E_{Hf} - N_N E_N \quad (2)$$

here, E_{CHfN} is grand energy for the heterojunction. E_C, is the carbon energy for the ground state, N_C is number of carbon atoms. E_{Hf}, grand energy for ground state of *Hf*, N_{Hf}, number of hafnium atoms, E_N, grand

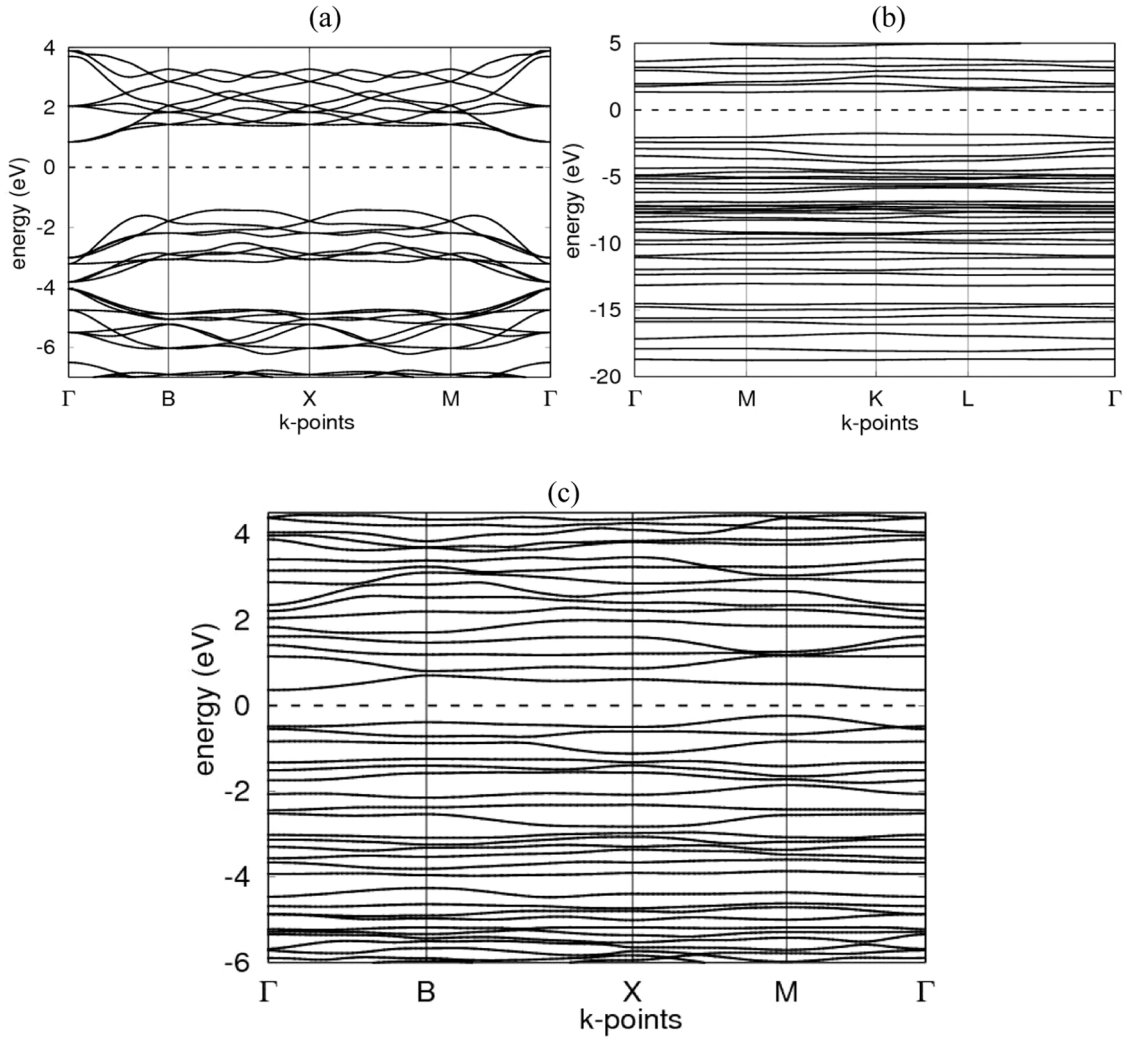

Fig. 2. Calculated band structures at high-symmetry k-points for (a) HfN2, (b) PVK and (c) HfN_2/PVK.

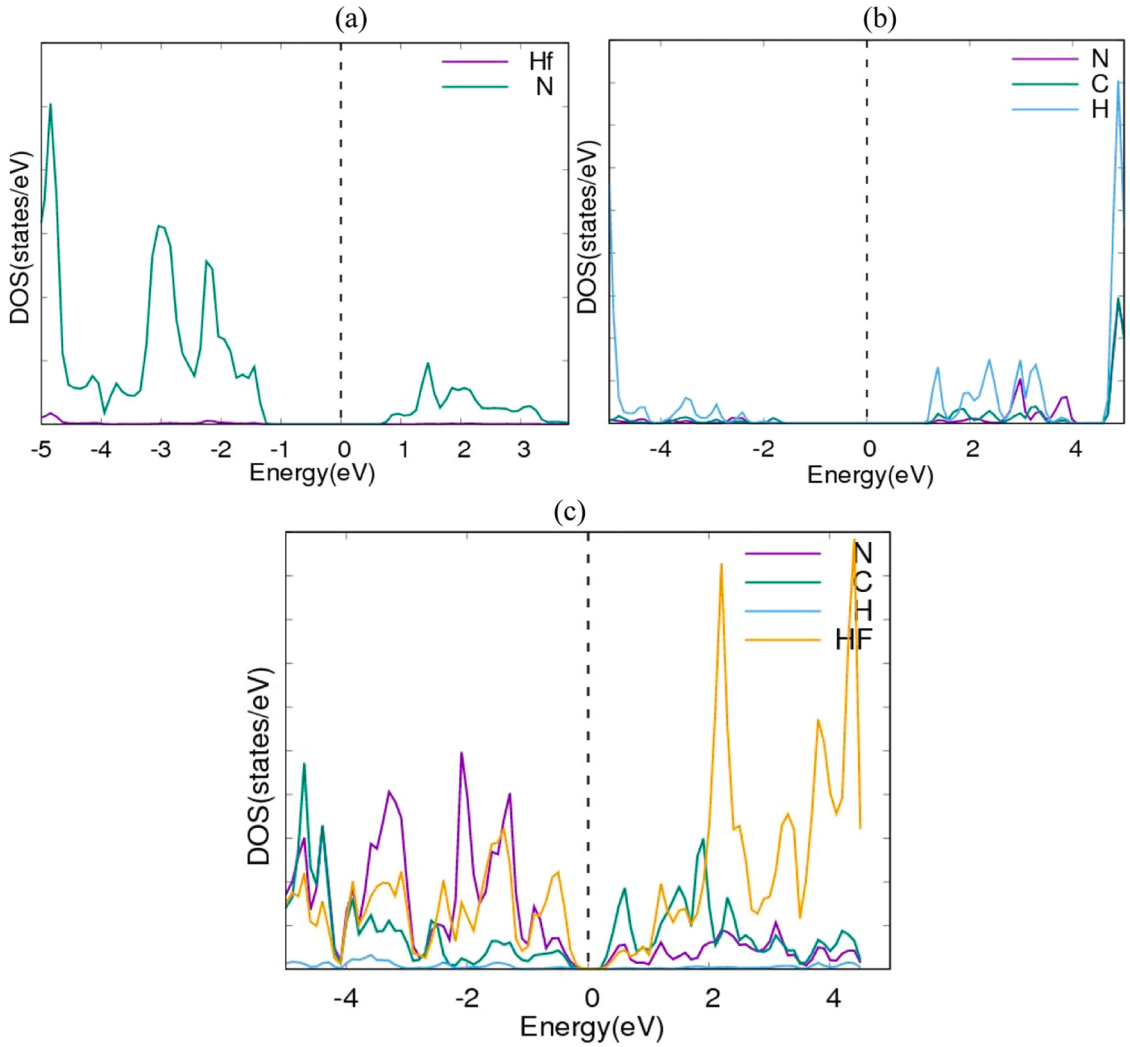

Fig. 3. DOS: (a) HfN2, (b) PVK, (c) HfN_2/PVK.

energy for N and N_N, nitrogen atoms count in the composite structure. Table 2 contains all the calculated formation energies per atom. All the calculated formation energies per atom are seen to be negative and large. This connotes the thermodynamic stability of the novel structure. Bond lengths computed before adsorption for N—N and N—Hf are 1.5145 and 2.2149 Å respectively. After adsorption the values calculated are 1.3951 and 2.1021 Å respectively. These are tabulated in Table 2. Comparison among energy of formation values in Table 3 reveals that PVK and HfN_2 structures have bigger values as compared to HfN_2/PVK. The interpretation is that the modeled structure has greater stability and thermodynamically favorable.

The modeled heterostructure can be easily obtained because it is energetically favorable and has stable configuration. The calculated binding energy between HfN_2 and PVK was found to be 22.43 meV/^{2}. This is comparable to van der Waals binding energy of 20 meV/Å^2 calculated in Refs. [61–63]. HfN_2/PVK therefore can be reasonably taken as a van der Waals heterostructure.

3.3. Electronic properties

Fig. 2(a–c) show the underlying band diagrams of HfN2, PVK and HfN_2/PVK respectively. The energy bandgap calculated for HfN_2 was 1.396 eV. This exhibited an indirect bandgap nature. In the case of PVK, the computed bandgap was 3.751 eV. This is a direct bandgap with both CBM and VBM situated at the Γ point. The gap value computed for the composite structure, HfN_2/PVK, was 0.958 eV. The heterojunction displayed an indirect energy gap. In this case, the CBM is situated at the Γ-point whilst the VBM is situated at an M-point, Fig. 2(c). For high efficiency energy conversion in solar cell and photovoltaic applications, the Γ-M indirect band-gap nature of the heterojunction commensurate any lattice dynamic mismatch. The indirect bandgap nature of the nanoheterointerface gives rise to enhancement of charge extraction and decline in charge recombination. It is expected that the blend will yield high carrier generation, low charge recombination and balanced charge transport based on the multi-length-scale morphology.

3.3.1. Photovoltaic performance of HfN_2/PVK interface

In this bulk heterojunction OSC, HfN_2 and PVK interfaces are stacked together to serve as active layers for efficient exciton diffusion and separation. The bulk heterojunction structure presents an enhanced donor-acceptor interface and reduces the diffusion distance for exciton separation, resulting in a significant improvement in device performance [64,65]. The blend of HfN_2/PVK interface offers an enhanced donor-acceptor interface and efficient exciton separation mechanism and is thereby expected to yield improved photocurrent and device performance.

The moieties of electron-rich and electron-deficient combinations leads to extended conjugation and decreased bandgap. This is what we have seen in Fig. 2(c). This will further increase the absorption of the active layers in the OSC. Donor material with a relatively low band gap

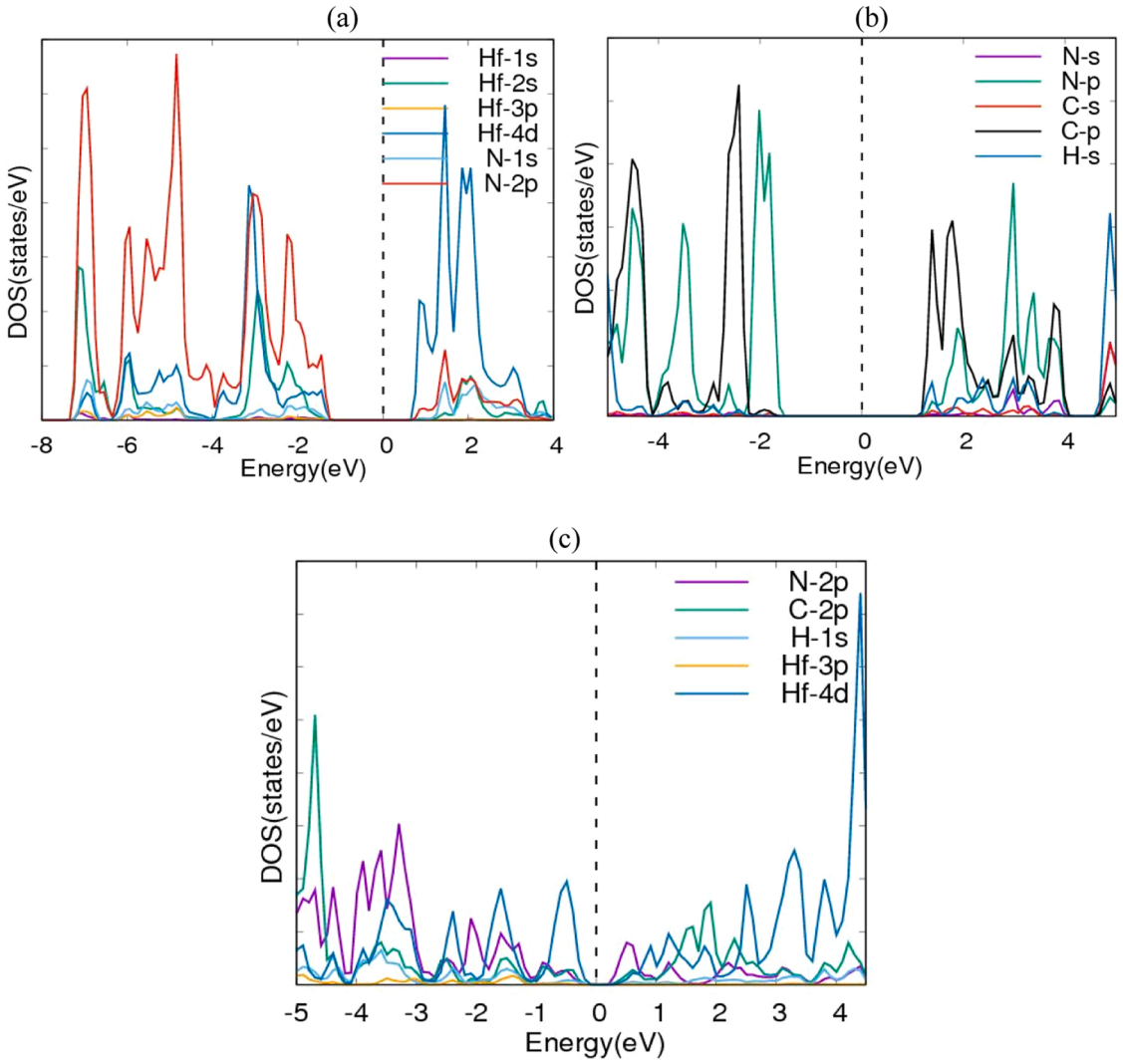

Fig. 4. PDOS: (a) HfN_2, (b) PVK monomer, (c) HfN_2/PVK.

is needed for efficient OSCs operation. HfN_2 as donor and PVK as acceptor enhance the absorption of the HfN_2/PVK blend to cover the solar spectrum from visible light to other levels. Under this condition, the LUMO–LUMO and HOMO–HOMO energy offsets are sufficient to induce free carrier generation at the heterojunction. HfN_2 affords a narrow bandgap of 1.396 eV and high absorption coefficient, thus the heterojunction is expected to facilitate improvement in conversion efficiency of photovoltaic power.

3.3.2. *Electronic density of states analysis*

Figs. 3–6 are the graphical representations of DOS, PDOS, DOS-TDOS plotted on the same axis and TDOS for HfN_2, PVK, HfN_2/PVK respectively. With the aid of the above pictorial representations, the nature of interactions and origin of energy gaps in the novel structure were analyzed. E_f, depicts Fermi energy level as zero in the band diagram as well as for the DOS diagrams. For HfN_2, it is seen that the DOS plot, Fig. 3(a), the PDOS plot, Fig. 4(a) and the valence band states are due to N 2p whilst the conduction band minimum is due to 4d-states of Hf atoms.

For PVK, the DOS plot, Fig. 3(b), the PDOS) plot, Fig. 4(b) and the valence band states are due to contributions from the N p-states while the conduction band minimum are due to contributions from C p-states.

For the HfN_2/PVK interface, the DOS plot, Fig. 3(c), the PDOS plot, Fig. 4(c) and the valence states are contribution from Hf 4d-states, the bottom of the conduction band is contributed by N 2p-states.

3.3.3. *Photocatalysis*

Characterization analysis of the band states suggests that the conduction band minimum and the valence band maximum are localized at separate monolayers in the HfN_2/PVK nanoheterostructure.

In the PVK monomer, the N p-states are responsible for the CBM whilst in the HfN_2, the Hf d-states are responsible for the VBM. Next, we calculated the band-decomposed charge density for both the CBM and the VBM at the Γ point. This procedure enabled us to analyze the significance of the component layers in the photocatalytic splitting of water in HfN_2/PVK heterointerface. From Fig. 4(c), the N-p orbitals dominate the LUMO and the HOMO is dominated by the Hf-d orbitals in the HfN_2/PVK heterointerface. PVK is the electron acceptor component in the HfN_2/PVK heterointerface whilst HfN_2 acts as the electron donor component. This means that the photoexcited electrons will migrate from the states localized in HfN_2 to the states localized in PVK during photocatalytic processes.

As such, production of hydrogen occurs within PVK component and oxygen production takes place in the HfN_2 component. The illustrated process in solar energy driven HfN_2/PVK splitting of water procedure is as demonstrated in Ref. [66]. As incident solar light is absorbed at the HfN_2/PVK heterointerface, there will be migration of photogenerated electrons from the VBM to the CBM. Therefore, H_2 and O_2 species will be

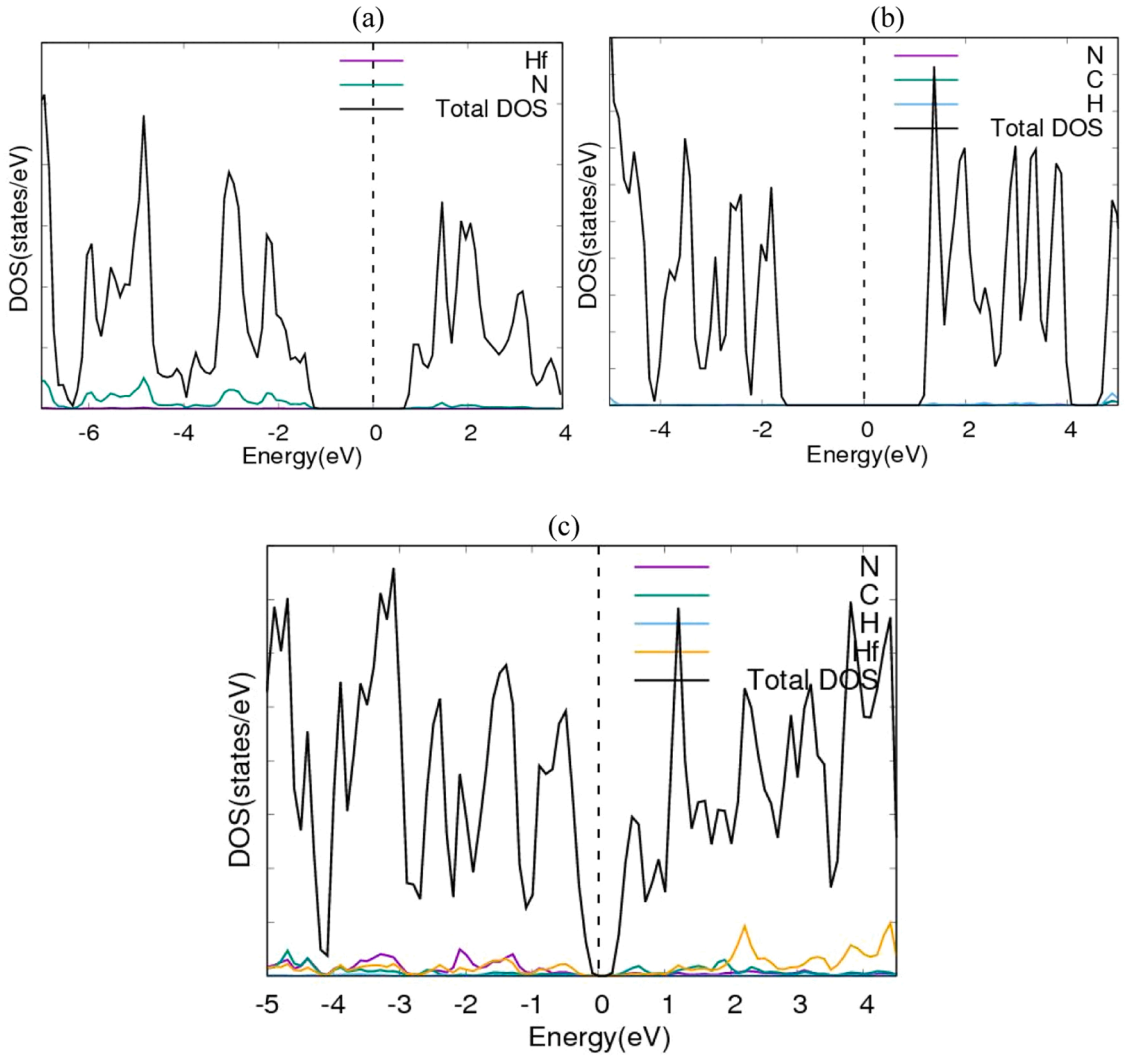

Fig. 5. DOS, TDOS combined: (a) HfN_2, (b) PVK monomer, (c) HfN_2/PVK.

liberated within PVK and HfN_2 compartments separately in photocatalytic water splitting.

3.3.4. *Charge transferred applying Lowdin technique*

Since the quantity of charge transferred comes with the calculational approach, we adopted the *Lowdin Charge Transfer* method. Under this method, the amount of charge transferred from PVK to HfN_2 was determined from the charge density projection onto the atomic orbitals. The value of the charge transferred was obtained as the difference between the Lowdin charges of the pure PVK and the HfN_2/PVK. This enabled as to ascertain the donor-acceptor character of the adsorbate molecule. The charge transferred between PVK and HfN_2 monomer in the HfN_2/PVK heterojunction was 0.85 electrons.

3.3.5. *Density of charge distribution*

Fig. 7 shows the charge density response application to internal electric field of HfN_2/PVK interface as obtained with Xcrysden software [67].

It is an established fact that polarization of surface charges directly influences atomic environment owning to the charge density distribution.

We observed significant differences in surface charge density spread between pure aromatic carbon polymers of the benzene ring and the π-conjugate planes of PVK. This is seen in close vicinity of the nitrogen heteroatom. In addition, there is a strong anisotropic polarizability as a result of surface charge distribution leading to relatively large response due to the π-conjugate plane of the polymer.

The partial density of states (PDOS) as shown in Fig. 3 indicates that Hf-4d and N-p states contributed mainly to the total density of state.

Similarly, in Fig. 7, the density of states distribution plots around Hf and N atoms show high concentration of charge density distribution. This is related to their comparable electronegativity values resulting in pulling of more electrons towards the atoms themselves for effective bonding.

3.3.6. *Charge density difference*

We have applied CDD methods to analyze the nature of the HfN_2/PVK interface. Charge Density Difference (CDD) is an essential analysis method.

The procedure measures differences within charge density among systems of interest, reference materials and the results are often plotted as charge redistribution. This redistribution shows the chemical bonds of the atomic species as depicted with areas of high concentration of residual charges. Our charge redistribution results showed that the interactions among hafnium atoms in the monomer and in the polymer points to the relevant phenomena to understand bonds between the two surfaces. The driving force behind the adhesion action is the degree of charge transfer between hafnium structure and the PVK monomer. This observation corroborates Lowdin charge transfer analysis. According to the CDD analyses in Fig. 8, the hafnium atoms of the monomer molecule

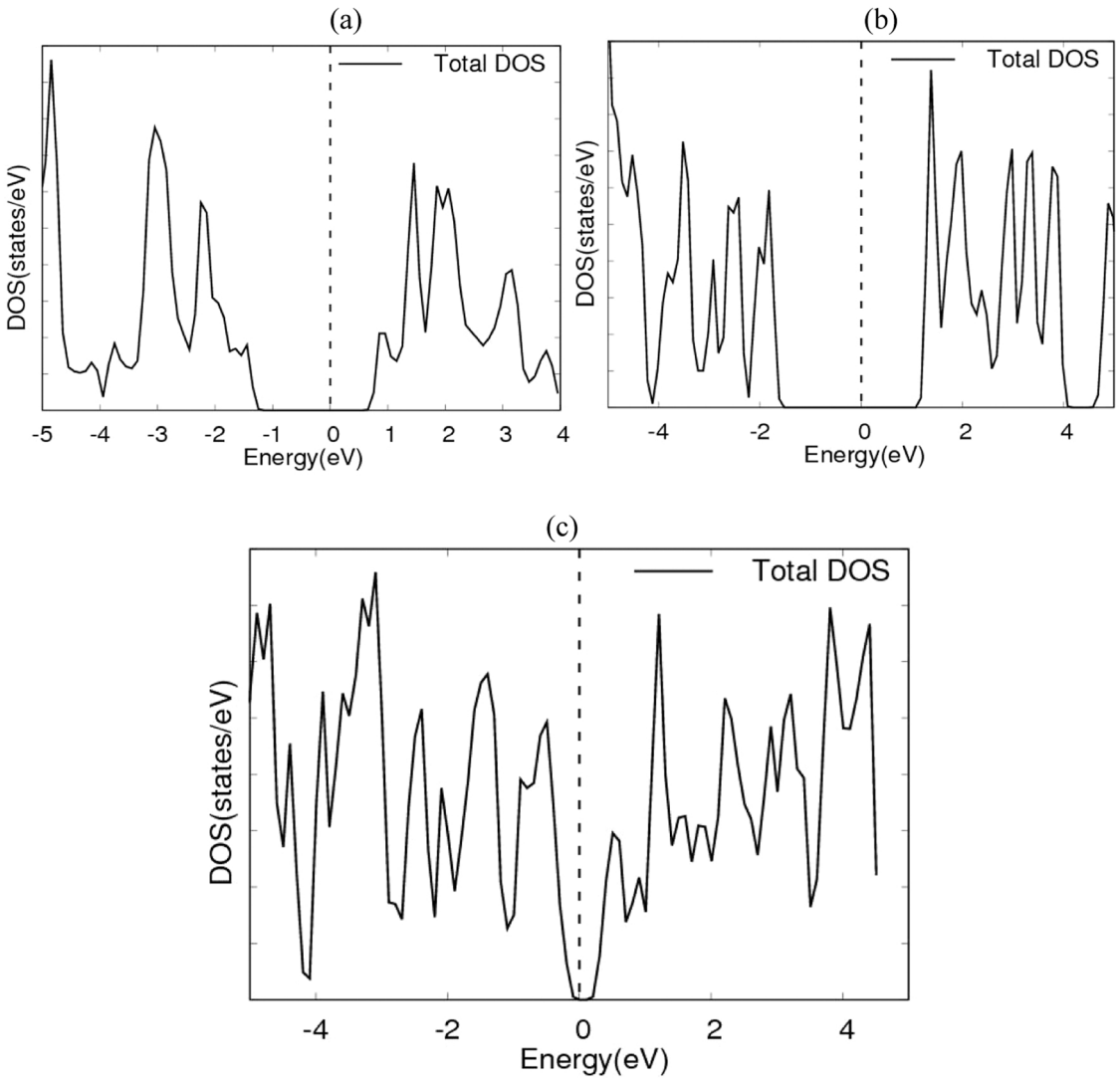

Fig. 6. Total DOS: (a) HfN_2, (b) PVK monomer, (c) HfN_2/PVK.

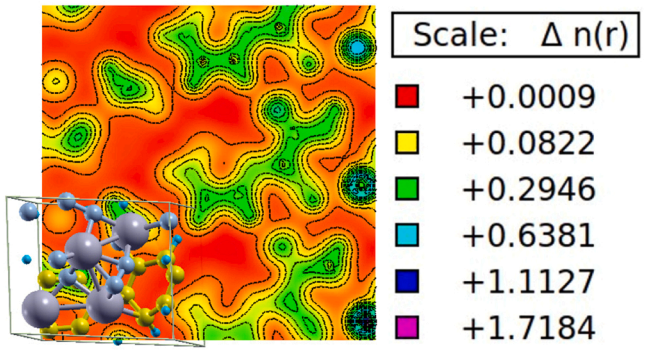

Fig. 7. Isolines-isosurfaces of HfN_2/PVK nanoarchitecture obtained from self-consistent field calculations. The color spectrum indicates maximum at purple side and decreases to pink as minimum charge density distribution.

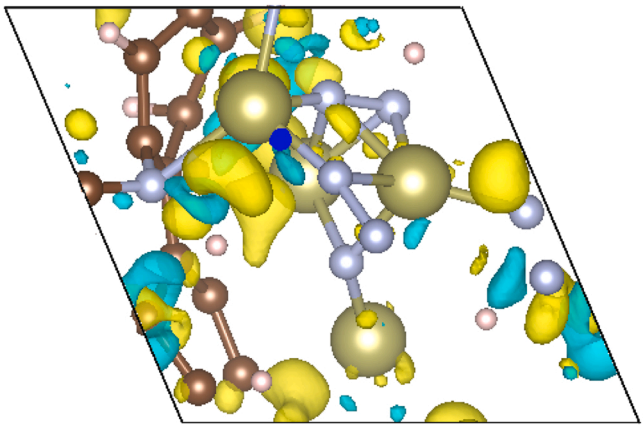

Fig. 8. Charge density difference (CDD) plot of HfN_2/PVK nanoheterojunction. The charge density difference shows the electron transfer between PVK and HfN_2 molecules. Yellow and cyan colors represent respectively positive and negative electronic charge densities.

gain electrons and become negatively charged while the atoms of the PVK molecule donate electrons and become positively charged.

3.3.7. *Optical properties*

Fig. 9(a–c) display optical spectral absorptions computed within pristine HfN_2, pristine PVK and HfN_2/PVK nanoheterojunction. Fig. 9(a)

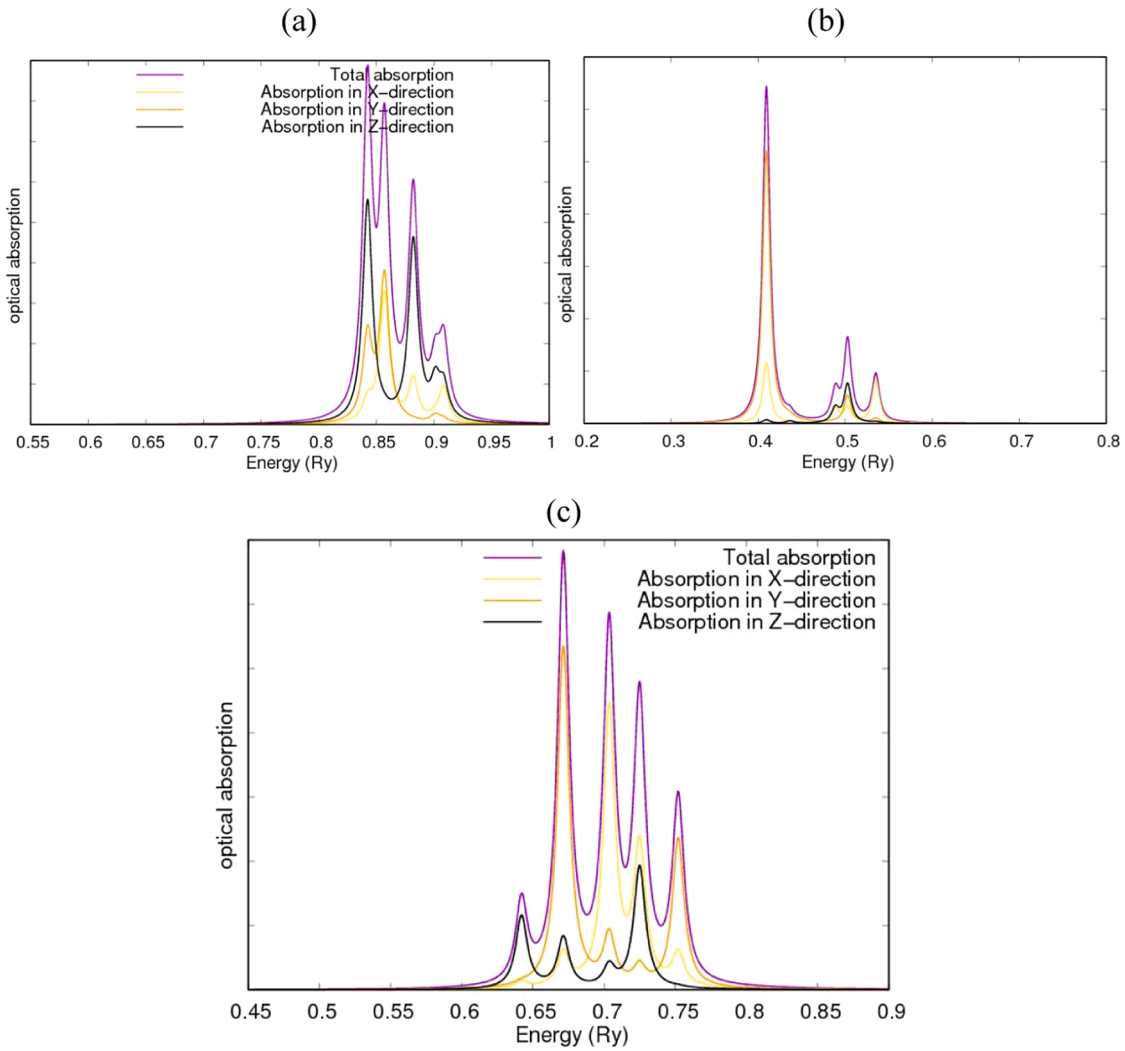

Fig. 9. Spectral optical absorption of (a) HfN_2, (b) PVK monomer and (c) HfN_2/PVK nanoheterojunction respectively.

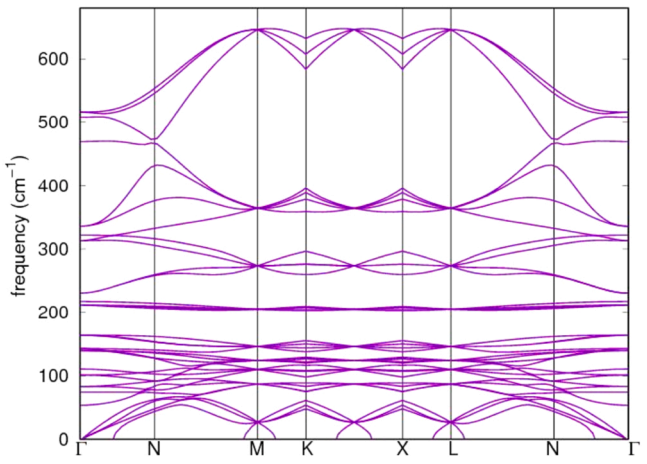

Fig. 10. Calculated phonon dispersion curves of HfN_2/PVK nanoheterojunction. A band-gap appearing in the phonon-spectra of HfN_2/PVK nanoheterojunction is evident.

depicts spectral absorption in HfN_2 excluding the PVK. Fig. 9(b) shows spectral absorption in PVK alone without the HfN_2. Fig. 9(c) portrays computed spectral absorption in the nanoheterojunction upon addition of PVK to HfN_2. 0.84, 0.85, 0.89, 0.91, 0.93 Ry are five intensity peaks observed in Fig. 9(a) with 0.84 Ry being the most pronounced. Intensity peaks manifested at 0.41, 0.43, 0.49, 0.51, 0.54 Ry in Fig. 9(b). 0.41 Ry being the most pronounced peak. It is evident from Fig. 9(c) that the addition of PVK to HfN_2 has caused quenching and shifting of the intensity peaks originally found in the pristine PVK and HfN_2 spectra. In Fig. 9(c), 0.64, 0.67, 0.71, 0.73, 0.76 Ry are the newly formed peaks. 0.67 Ry was observed as the most intensity peak. The appearance of new peaks at different positions in the complex portrays processes of charge transfer taking place between PVK and HfN_2 structures.

3.3.8. *Phonon dispersion analysis*

The dispersion relations of the phonon calculations of HfN_2/PVK nanoheterojunction interface in the Irreducible BZ is shown in Fig. 10. The dynamical matrices were computed along the high symmetry points $\Gamma - N - M - L - \Gamma$. The dynamical matrices at the BZ were obtained using the Fourier interpolation scheme. We observed energy gap between the low-frequency and the high-frequency phonons which could be attributed to stretching originating from the symmetric and antisymmetric stretching modes in the supercell. The soft modes are positive indicating that the interfacial structure of the heterostructure is stable and consistent with earlier experimental results of Baibarac and coworkers [68].

The figure further shows that the highest phonon branches are clearly separated from the lower branches without any degeneracy. Strong dispersive relation exists between the highest and the lowest

branches. The transverse acoustic (TA) vibrations belong to the low-frequency modes whilst those of the longitudinal acoustic (LA) vibrations belong to the high-frequency modes and all the collective modes of vibrations originate from the C-atoms. Similarly, optical modes with higher frequencies are associated with the N-atoms lattice vibrations.

We observed again that, the HfN_2/PVK phonon dispersion has its longitudinal optical (LO) and transverse optical (TO) modes splitting up at the Γ-point as a consequence of the long-range diploe order interaction usually associated with semiconductor and insulator polar materials. Notwithstanding, the relatively large atomic mass difference between Hf and N atoms creates gaps which is revealed in the region between the dominant acoustic and optical branches modes respectively because of the relative displacements between the atoms accordingly. The calculated dispersion for HfN_2/PVK is in good agreement with experimental observations [69]. Nevertheless, our calculated phonon dispersion compares quite well with calculations of Isaev and colleagues [70] and Heid's group [71].

4. Conclusions

In conclusion, we have presented a comparative first principles theoretical analysis of structural, electronic, optical and vibrational properties of HfN_2 and PVK, with a motivation to assess their potential for optoelectronic applications. While HfN_2 is a transition metal dinitride with a small indirect electronic band gap, PVK is a conjugated polymer exhibiting a large indirect band gap. HfN_2/PVK nanoheterointerface has a narrow indirect energy gap. The HfN_2/PVK nanoheterojunction exhibits very good optical absorption characteristics in the visible-light wavelengths where HfN_2 and PVK act as electron donor and electron acceptor respectively. This character will facilitate the efficient separation and transportation of the photogenerated charges and thus increase the efficiency of the photocatalytic processes. Combining the effective migration and separation of carriers, the new heterointerface has a great possibility to be used as a photocatalyst for overall water splitting. Our study highlights the applications of heterointerfaces as photocatalysts and provides useful guidance to further expand the practical application range of hybrid materials.

Appreciation

We appreciate the freewill of CHPC for availing the Lengau computer-cluster to us. We are very grateful.

Declaration of Competing Interest

The authors declare that they have no known competing financial interests or personal relationships that could have appeared to influence the work reported in this paper.

References

[1] N. Koch, Organic electronic devices and their functional interfaces, Chem. Phys. Chem. 8 (2007) 1438–1455.
[2] T.W. Tang, 2-Layer organic photovoltaic cell, Appl. Phys. Lett. 48 (1986) 183–185.
[3] Y. Cui, H.F. Yao, Y. Xu, 100 cm^2 organic photovoltaic cells with 23 % efficiency under indoor illumination, Chin. J. Polym. Sci. 40 (2022) 979–988, https://doi.org/10.1007/s10118-022-2761-x.
[4] K. Jin, Z. Xiao, L. Ding, 18.69 % PCE from organic solar cells, J. Semicond. 42 (2021) 060502, https://doi.org/10.1088/1674-4926/42/6/060502.
[5] W. Peng, Over 18 % ternary polymer solar cells enabled by a terpolymer as the third component, Nano Energy 92 (2022) 106681, https://doi.org/10.1016/j.nanoen.2021.106681.
[6] M. Zhang, Single-layered organic photovoltaics with double cascading charge transport pathways: 18 % efficiencies, Nat. Commun. 12 (2021) 309, https://doi.org/10.1038/s41467-020-20580-8.
[7] Y. Cui, Single-junction organic photovoltaic cell with 19 % efficiency, Adv. Mater. 33 (2021) 2102420, https://doi.org/10.1002/adma.202102420.
[8] K. Chong, Realizing 19.05 % efficiency polymer solar cells by progressively improving charge extraction and suppressing charge recombination, Adv. Mater. 34 (2022) 2109516, https://doi.org/10.1002/adma.202109516.
[9] G. Li, Non-fullerene acceptors with direct and indirect hexa-fluorination afford > 17 % efficiency in polymer solar cells, Energy Environ. Sci. 15 (2022) 645–659, https://doi.org/10.1039/D1EE03225A.
[10] H. Chen, A guest-assisted molecular-organization approach for > 17 % efficiency organic solar cells using environmentally friendly solvents, Nat. Energy 6 (2021) 1045–1053, https://doi.org/10.1038/s41560-021-00923-5.
[11] X. Kong, 18.55 % efficiency polymer solar cells based on a small molecule acceptor with alkylthienyl outer side chains and a low-cost polymer donor PTQ10, CCS Chem. 22 (2022) 2056, https://doi.org/10.31635/ccschem.022.202202056.
[12] Y. Cui, Single-junction organic photovoltaic cells with approaching 18 % efficiency, Adv. Mater. 32 (2020) 1908205, https://doi.org/10.1002/adma.201908205.
[13] L. Zhan, Over 17 % efficiency ternary organic solar cells enabled by two non-fullerene acceptors working in an alloy-like model, Energy Environ. Sci. 13 (2020) 635–645, https://doi.org/10.1039/C9EE03710A.
[14] L. Zhan, Desired open-circuit voltage increase enables efficiencies approaching 19 % in symmetric-asymmetric molecule ternary organic photovoltaics, Joule 6 (2022) 662–675, https://doi.org/10.1016/j.joule.2022.02.001.
[15] L. Zhu, Single-junction organic solar cells with over 19 % efficiency enabled by a refined double-fibril network morphology, Nat. Mater. 21 (2022) 656–663, https://doi.org/10.1038/s41563-022-01244-y.
[16] F. Zhao, Single-junction binary-blend non-fullerene polymer solar cells with 12.1 % efficiency, Adv. Mater. 29 (2017) 1700144, https://doi.org/10.1002/adma.201700144.
[17] W. Zhao, Fullerene-free polymer solar cells with over 11 % efficiency and excellent thermal stability, Adv. Mater. 28 (2016) 4734–4739, https://doi.org/10.1002/adma.201600281.
[18] J. Yuan, Single-junction organic solar cell with over 15 % efficiency using fused-ring acceptor with electron-deficient core, Joule 3 (2019) 1140–1151, https://doi.org/10.1016/j.joule.2019.01.004.
[19] X. Chen, Realizing ultrahigh mechanical flexibility and > 15 % efficiency of flexible organic solar cells via a "welding" flexible transparent electrode, Adv. Mater. 32 (2020) 1908478, https://doi.org/10.1002/adma.201908478.
[20] G. Zeng, Breaking 12 % efficiency in flexible organic solar cells by using a composite electrode, Sci. China Chem. 62 (2019) 851–858, https://doi.org/10.1007/s11426-018-9430-8.
[21] Shailesh Narain Sharma, Parul Chawla, Akanksha, A.K. Srivastava, Physica E 80 (2016) 101–107.
[22] Tingting Zheng, Jiayue Xu, Zhijie Zhang, Haibo Zeng, Mater. Lett. 164 (2016) 640–643.
[23] W. Jaimes, G. Alvarado-Tenorio, Claudia Martínez-Alonso, A. Quevedo-López, Hailin Hu, M.E. Nicho, Mater. Sci. Semicond. Process. 37 (2015) 259–265.
[24] Alena S. Kalyakina, Valentina V. Utochnikova, Elena Yu Sokolova, Andrey A. Vashchenko, Leonid S. Lepnev, Rik Van Deun, Alexander L. Trigub, Yan V. Zubavichus, Michael Hoffmann, Susan Mühl, Natalia P. Kuzmina, Org. Electron. 28 (2016) 319–329.
[25] Andrey N. Aleshin, Igor P. Shcherbakov, Alexei S. Komolov, Vasily N. Petrov, Irina N. Trapeznikova, Org. Electron. 16 (2015) 186–194.
[26] Shurong Wang, Yanfei Kang, Liwei Wang, Hongxin Zhang, Yanshuang Wang, Yao Wang, Sens. Actuators B, vol. 182, 2013, pp. 467–81.
[27] Hana Faltakh, Mounira Mahdouani, Issam Hemdana, Sadok Ben Dkhil, Ramzi Bourguiga, Joel Davenas, Superlattices Microstruct. 79 (2015) 166–179.
[28] S.Ben Dkhil, J. Davenas, R. Bourguiga, D. Cornu, Synth. Met. 161 (2011) 1928–1933.
[29] Antonio Guerrero, Emilio J. Juarez-Perez, Juan Bisquert, Ivan Mora-Sero, Germa Garcia-Belmonte, Appl. Phys. Lett. 105 (2014) 133902–133907.
[30] Tzong-Liu Wang, Chien-Hsin Yang, Yeong-Tarng Shieh, An-Chi Yeh, ChinHsiang Chen, Tsung-Han Ho, Mater. Chem. Phys. 132 (2012) 131–137.
[31] V.W. Elloh, E.Okoampa Boadu, D. Abbeyquaye, D.E. Anderson, A. Yaya, Photocatalytic enhancement mechanisms for novel g-C3N4/ PVK nanoheterojunction, Mater. Chem. Phys. 296 (2023) 127275, https://doi.org/10.1016/j.matchemphys.2022.127275.
[32] Van Wellington Elloh, Gebremedhn Gebreyesus, Kwabena Kan-Dapaah, Edwin Okoampa Boadu, Eric Kwabena Kyeh Abavare, David Ebo Anderson, Daniel Abbeyquaye, Isaac Arhin, Felix Djan Ofosuhene, Abhishek Kumar Mishra, David Dodoo-Arhin, Abu Yaya, Poly(9-vinylcarbazole)/graphene nanoheterostructure interfaces: ab initio dynamics studies for photovoltaic and optoelectronic applications, Biointerface Res. Appl. Chem. 13 (2023) 399, https://doi.org/10.33263/BRIAC134.399.
[33] J.P. Perdew, K. Burke, M. Ernzerhof, Phys. Rev. Lett. 77 (1996) 3865.
[34] X. Hua, X. Chen, W.A. Goddard III, Phys. Rev. B 55 (1997) 16103.
[35] D. Vanderbilt, Phys. Rev. B 41 (1990) 7892.
[36] H.J. Monkhorst, J.D. Pack, Phys. Rev. B 13 (1976) 5188.
[37] M. Methfessel, A. Paxton, Phys. Rev. B 40 (1989) 3616.
[38] P. Giannozzi, O. Andreussi, T. Brumme, O. Bunau, M. Buongiorno, Advanced capabilities for materials modelling with Quantum ESPRESSO, J. Phys. Condens. Matter 29 (2017).
[39] S. Baroni, S. de Gironcoli, A.D. Corso, P. Giannozzi, Rev. Mod. Phys. 73 (2001) 515.
[40] V.S. Bhadram, D.Y. Kim, T.A. Strobel, High-pressure synthesis and characterization of incompressible titanium pernitride, Chem. Mater. 28 (2016) 1616–1620.
[41] S. Yu, Q. Zeng, A.R. Oganov, G. Frapper, L. Zhang, Phase stability, chemical bonding and mechanical properties of titanium nitrides: a first-principles study, Phys. Chem. Chem. Phys. 17 (2015) 11763–11769.
[42] M.B. Takeyama, M. Sato, E. Aoyagi, A. Noya, Preparation of nanocrystalline HfNx films as a thin barrier for through-Si via interconnects in three-dimensional integration, Jpn. J. Appl. Phys. 53 (2014) 02BC05.

[43] Y. Sun, B. Xu, L. Yi, HfN2 monolayer: a new direct-gap semiconductor with high and anisotropic carrier mobility, Chin. Phys. B 29 (2020) 23102.
[44] M.K. Mohanta, A. Rawat, A. De Sarkar, Atomistic manipulation of interfacial properties in HfN2/MoTe2 van der Waals heterostructure via strain and electric field for next generation multifunctional nanodevice and energy conversion, Appl. Surf. Sci. 568 (2021) 150928.
[45] M.K. Mohanta, I.S. Fathima, A. De, Sarkar, Exceptional mechano-electronic properties in the HfN2 monolayer: a promising candidate in low-power flexible electronics, memory devices and photocatalysis, Phys. Chem. Chem. Phys. 22 (2020) 21275–21287.
[46] M.K. Mohanta, A. De Sarkar, 2D HfN2/graphene interface based Schottky device: unmatched controllability in electrical contacts and carrier concentration via electrostatic gating and out-of-plane strain, Appl. Surf. Sci. 540 (2021) 148389.
[47] B. Zhai, R. Cheng, W. Yao, L. Yin, C. Shen, C. Xia, J. He, Using ferroelectric polarization to regulate and preserve the valley polarization in a HfN2/CrI3/In2Se3 Heterotrilayer, Phys. Rev. B 103 (2021) 214114.
[48] M.K. Mohanta, A. De, Sarkar, Coupled spin and valley polarization in monolayer HfN2 and valley-contrasting physics at the HfN2−WSe2 interface, Phys. Rev. B 102 (2020) 125414.
[49] J.M. Pearson, M. Stolka, Poly(N-vinylcarbazole). Polymer Monographs, Gordon and Breach, New York, 1981 (vol. 6. ISBN: 0-677-05520-X).
[50] J.M. Pearson, Vinyl carbazole polymers, in: H.F. Mark, N. Bikales, C.G. Overberger, G. Menges (Eds.), Encyclopedia of Polymer Science and Engineering, 2nd ed., Wiley Interscience, New York, 1989, pp. 257–294.
[51] J.V. Grazulevicius, P. Strohriegl, J. Pielichowski, K. Pielichowski, Carbazole-containing polymers: synthesis, properties and applications, Prog. Polym. Sci. 28 (9) (2003) 1297–1353.
[52] M.D. Shattuck, U. Vahtra, Organic photoconductive compositions and their use in electrophotographic processes, US patent 3 484 237, assigned to International Business Machine Corporation, Armonk, NY, 1969.
[53] D.J. Hans, K. Ruth, Koordinatoren: Lexikon der Chemie In drei Bänden, Spektrum Verl. Heidelb. 3 (1999) 92.
[54] Naoto Tsutsumi, Molecular design of photorefractive polymers, Polym. J. 48 (2016) 571–588.
[55] Y. Wang, N. Herron, J. Lumin, Poly(N-vinylcarbazole) (PVK) photoconductivity enhancement induced by doping with CdS nanocrystals through chemical hybridization, J. Phys. Chem. B70 (2000) 48.
[56] D. Mombru, Microstructure evolution, thermal stability and fractal behaviour of water vapor flow assisted in situ growth poly (vinylcarbazole)-titania quantum dots nanocomposites, J. Phys. Chem. Solids 111 (2017) 199–206.
[57] R. Liu, Noncovalent functionalization of carbon nanotube using poly (vinylcarbazole)-based compatibilizer for reinforcement and conductivity improvement in epoxy composite, J. Appl. Polym. Sci. 134 (2017) 199–206.
[58] G.E. Hans, Poly(N-vinylcarbazol), 3, in: Hans-Georg Elias (Ed.), Makromoleküle Industrielle Polymere und Synthesen, Wiley-VCH, Weinheim, 2001, p. 211.
[59] X.L. Hu, Y.F. Zhang, N.F. Zhuang, J. Q. Qian, J. Sol. Stat. Chem. 183 (2010) 2741.
[60] B. Zhai, R. Cheng, W. Yao, L. Yin, C. Shen, C. Xia, J. He, Using ferroelectric polarization to regulate and preserve the valley polarization in a HfN2/CrI3/In2Se3 heterotrilayer, Phys. Rev. B 103 (21) (2021), https://doi.org/10.1103/PhysRevB.103.214114.
[61] T. Bjo¨rkman, A. Gulans, A.V. Krasheninnikov, R.M. Nieminen, Van der Waals bonding in layered compounds from advanced density-functional first-principles calculations, Phys. Rev. Lett. 108 (2012) 235502–235507.
[62] H.U. Din, M. Idrees, Q. Alam, B. Amin, Van der Waal heterostructure based on BY (Y As, P) and MX2 (M Mo, W; X S, Se) monolayers, Appl. Surf. Sci. 568 (2021) 150846, https://doi.org/10.1016/j.apsusc.2021.150846.
[63] H. Zhao, F. Xie, Y. Liu, B. Bian, G. Yang, Y. Ding, X. Gu, Van der Waals heterostructures of Janus XSeTe (X = Mo, W) and arsenene monolayers: a first principles study, Mater. Sci. Semicond. Process. 123 (2021) 105588, https://doi.org/10.1016/j.mssp.2020.105588.
[64] Z. Zheng, J. Wang, P. Bi, J. Ren, Y. Wang, Y. Yang, X. Liu, S. Zhang, J. Hou, Tandem organic solar cell with 20.2 % efficiency, Joule 6 (2022) 171–184.
[65] G. Yu, J. Gao, J.C. Hummelen, F. Wudl, A.J. Heeger, Polymer photovoltaic cells: enhanced efficiencies via a network of internal donor-acceptor heterojunctions, Science 270 (1995) 1789.
[66] J. Liao, B. Sa, J. Zhou, R. Ahuja, Z. Sun, Design of high-efficiency visible-light photocatalysts for water splitting: MoS_2/AlN(GaN) heterostructures, J. Phys. Chem. C 118 (2014) 17594–17599.
[67] A. Kokalj, Computer graphics and graphical user interfaces as tools in simulations of matter at the atomic scale, Comp. Mater. Sci. 28 (2003) 155–168.
[68] M. Baibarac, I.S. Baltog, P. Lefrant, Gomez-Romero, Spectroscopic evidence for the bulk polymerization of N-vinyl carbazole in the presence of single-walled carbon nanotubes, Polymer 48 (2007) 5279–5288, https://doi.org/10.1016/j.polymer.2007.07.008.
[69] S. Duman, S. Bagci, H.M. Tutuncu, G. Ugur, G.P. Srivastava, Diamond Relat. Mater. 15 (2006) 1175.
[70] E.I. Isaev, S.I. Simak, I.A. Abrikosov, R. Ahuja, Y.K. Vekilov, M.I. Katsnelson, A. I. Lichtenstein, B. Johansson, J. Appl. Phys. 101 (2007) 123519.
[71] R. Heid, K.-P. Bohnen, B. Renker, T. Wolf, H. Schober, Phys. Rev. B 71 (2005) 092302.